

Multiplet of skyrmion states on a curvilinear defect: skyrmion lattices as a ground state

Volodymyr P. Kravchuk,^{1,2,*} Denis D. Sheka,³ Oleksii M. Volkov,⁴

Ulrich K. Rößler,² Jeroen van den Brink,^{2,5} Denys Makarov,⁴ and Yuri Gaididei¹

¹*Bogolyubov Institute for Theoretical Physics of National Academy of Sciences of Ukraine, 03680 Kyiv, Ukraine*

²*Leibniz-Institut für Festkörper- und Werkstoffsorschung, IFW Dresden, D-01171 Dresden, Germany*

³*Taras Shevchenko National University of Kyiv, 01601 Kyiv, Ukraine*

⁴*Helmholtz-Zentrum Dresden-Rossendorf e.V., Institute of Ion Beam Physics and Materials Research, 01328 Dresden, Germany*

⁵*Institute for Theoretical Physics, TU Dresden, 01069 Dresden, Germany*

(Dated: October 2, 2018)

We show that the presence of a localized curvilinear defect drastically changes magnetic properties of a thin perpendicularly magnetized ferromagnetic film. For a large enough defect amplitude a discrete set of equilibrium magnetization states appears forming a ladder of energy levels. Each equilibrium state has either zero or unit topological charge, i.e. topologically trivial and skyrmion multiplets generally appear. Transitions between the levels with the same topological charge are allowed and can be utilized to encode and switch a bit of information. There is a wide range of geometrical and material parameters, where the skyrmion level has the lowest energy. As a result a periodically arranged curvilinear defects generate a skyrmion lattice as the ground state.

PACS numbers: 75.10.Hk, 75.10.Pq, 75.40.Mg, 75.60.Ch, 75.78.Cd, 75.78.Fg

I. INTRODUCTION

An isolated magnetic chiral skyrmion is a localized topologically nontrivial excitation, which may appear in a perpendicularly magnetized ferromagnetic film, when the Dzyaloshinskii-Moriya interaction (DMI) is present.^{1–3} During the last years isolated skyrmions have been widely considered as data carriers in spintronic data storage and logic devices of a racetrack configuration.^{3–10} Besides nanotracks^{3–5,11,12} individual skyrmions were obtained in nanodisks.^{5,13,14} Due to nonlocal magnetostatic effects in confined magnetic objects, the skyrmion state can have lower energy as compared to the topologically trivial homogeneous state.^{5,13}

In contrast to individual skyrmions, their periodic 2D arrays, i.e. skyrmion lattices^{15–19} are relevant for electronics relying on topological properties of materials. In this regard, dense lattices of small-sized skyrmions facilitate the signal readout in prospective spintronic devices by enhancing the topological Hall effect.^{20–23} Typically, skyrmion lattices are in-field low temperature pocket phases^{15–18} which hinder their application potential.

Here we demonstrate that magnetic skyrmion can be pinned on a localized curvilinear defect and can have two or more equilibrium states with very different skyrmion radius, i.e. one deals with a multiplet of skyrmion states. In this context, a doublet of skyrmion states can be used to represent a single bit of information, see Fig. 1(b). This unique feature of a skyrmion on a curvilinear defect paves the way towards a new memory concept which is based on immobile skyrmions.

It is remarkable that when the radii of the skyrmion and the curvilinear defect are comparable, the energy of the skyrmion state can be the lowest one within the class of radially symmetrical solutions. In this way we

demonstrate the possibility to realize the lowest energy skyrmion states on a curvilinear defect relying on local interactions only without the need of any magnetic field or magnetostatic effects. As a consequence, a periodically arranged lattice of the defects can generate a skyrmion lattice as a ground state, see Fig. 1(c). It is important that such a skyrmion lattice exists in zero magnetic field and for a temperature regime, which allows individual skyrmions, e.g. for room temperatures.^{12,24} In contrast to the planar case^{25,26} the proposed zero-field lattice does not require four-spin interactions, it can have an arbitrary symmetry and its length scale can be much larger than atomic one. The proposed static reconfigurable lattice of skyrmions opens new exciting perspective for the manipulation and control of spintronic devices relying on the topological Hall effect.^{20–23} Moreover, the feature of the reconfigurability of the lattice enables new functionality for the skyrmion-based neural network devices.^{27–29}

II. MODEL

Similarly to the well studied planar case^{2,30–34} the form of a chiral skyrmion is mainly determined by competition of three local interactions: exchange, easy-normal anisotropy and DMI. Thus the energy functional of our model reads

$$E = L \int [A\mathcal{E}_{\text{ex}} + K(1 - m_n^2) + D\mathcal{E}_{\text{D}}] dS, \quad (1)$$

here L is the film thickness and the integration is performed over the film area. The first term of the integrand is the exchange energy density with $\mathcal{E}_{\text{ex}} = \sum_{i=x,y,z} (\partial_i \mathbf{m})^2$, and A being the exchange constant. Here $\mathbf{m} = \mathbf{M}/M_s$ is the unit magnetization vector

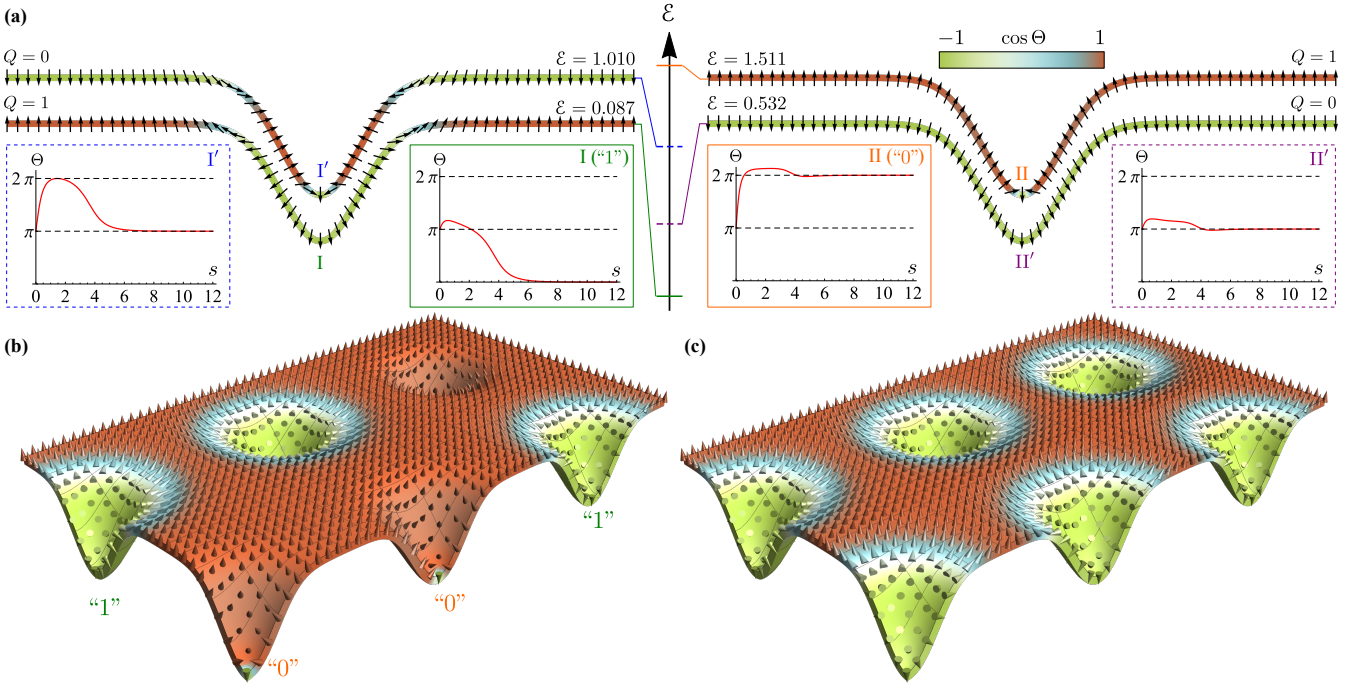


FIG. 1. Individual skyrmion profiles and skyrmion lattices. (a): Equilibrium magnetization states of a Gaussian concave bump ($\mathcal{A} = -3$, $r_0 = 1$ and $d = 1$) are shown by means of vertical cross-sections. Arrows show the magnetization distribution and color corresponds to the normal component $m_n = \cos \Theta$. The corresponding solutions $\Theta(s)$ of Eq. (3) are shown in the insets I, II, I' and II'. Vertical axis \mathcal{E} shows distribution of the corresponding energy levels obtained from (4). (b): Two skyrmion states with big (I) and small (II) radii are shown on the same bumps arranged in a square lattice. These skyrmion solutions can be considered as logical states “1” and “0” of an information bit. (c) Skyrmion lattice as a ground state.

with M_s being the saturation magnetization. The second term is the easy-normal anisotropy where $K > 0$ and $m_n = \mathbf{m} \cdot \mathbf{n}$ is the normal magnetization component with \mathbf{n} being the unit normal to the surface. The exchange-anisotropy competition results in the magnetic length $\ell = \sqrt{A/K}$, which determines a length scale of the system. The last term in (1) represents DMI with $\mathcal{E}_D = m_n \nabla \cdot \mathbf{m} - \mathbf{m} \cdot \nabla m_n$. Such a kind of DMI originates from the inversion symmetry breaking on the film interface; it is typical for ultrathin films^{33,35,36} or bilayers,³⁷ and it results in so called Néel (hedgehog) skyrmions.^{5,38} For a surface of rotation with a radially symmetrical magnetization distribution the same type of DMI effectively appears in the exchange term due to curvature effects,^{39–41} thus a direct competition takes place. This results in a skyrmion solution of Néel type. Another types of DMI may lead to a spiral-like skyrmion, which are intermediate ones between Néel and Bloch types. This case would require a more bulk analysis.

In our model we disregard nonlocal magnetostatic effects. Still, in stark contrast to the planar case, this is not required for the realization of a skyrmion lowest energy state.⁴² We also assume magnetization homogeneity along the normal direction, which is valid for $L \lesssim \ell$.

We now consider a curvilinear defect of the film, which is formed by a complete revolution of the curve $\gamma = r\mathbf{e}_x + z(r)\mathbf{e}_z$ around z -axis – a bump, see Appendix A for

details. The parameter $r \geq 0$ denotes the distance to the axis of rotation. The surface is assumed to be smooth everywhere, thus $z'(0) = 0$. Here and below all distances are considered dimensionless and they are measured in units of the magnetic length ℓ . Curvilinear properties of the surface at each point are completely determined by two principal curvatures k_1 and k_2 , see the explicit forms in Appendix A.

The constrain $|\mathbf{m}| = 1$ is utilized by introducing the spherical angular parameterization $\mathbf{m} = \sin \theta \cos \phi \mathbf{e}_s + \sin \theta \sin \phi \mathbf{e}_\chi + \cos \theta \mathbf{n}$ in the local orthonormal basis $\{\mathbf{e}_s, \mathbf{e}_\chi, \mathbf{n}\}$, where \mathbf{e}_s is unit vector tangential to the curve γ , and $\mathbf{e}_\chi = \mathbf{n} \times \mathbf{e}_s$ is the unit vector in azimuthal direction, see Fig. 4. Expressions for \mathcal{E}_{ex} and \mathcal{E}_D for a general case of a local curvilinear basis were previously obtained in Ref. 39 and Ref. 41, respectively. Without edge effects (e.g. for a closed surface or for an infinitely large film) the DMI energy density can be reduced to the form

$$\mathcal{E}_D = \sin^2 \theta [2(\nabla \theta \cdot \boldsymbol{\varepsilon}) + \mathcal{H}], \quad (2)$$

where $\boldsymbol{\varepsilon} = \cos \phi \mathbf{e}_s + \sin \phi \mathbf{e}_\chi$ is normalized projection of the vector \mathbf{m} on the tangential plane and $\mathcal{H} = k_1 + k_2$ is the mean curvature. Expression (2) clearly shows the appearance of an effective DMI-driven uniaxial anisotropy proportional to the mean curvature. It has the same curvilinear origin as the recently obtained exchange-

driven anisotropy and DMI.^{39,40} Depending on sign of the product $D\mathcal{H}$ this anisotropy can be of easy-normal ($D\mathcal{H} > 0$) or easy-surface ($D\mathcal{H} < 0$) type.⁴³

One can show (see Appendix B) that the total energy (1) is minimized by a stationary solution $\mathbf{m} = \sin\Theta\mathbf{e}_s + \cos\Theta\mathbf{n}$, where function $\Theta(s) \in \mathbb{R}$ is determined by equation

$$\Delta_s\Theta - \sin\Theta\cos\Theta\Xi + \frac{r'}{r}(d - 2k_2)\sin^2\Theta = \mathcal{H}'. \quad (3)$$

Here s is the arc length along γ . The radial part of the Laplace operator reads $\Delta_s f = r^{-1}(rf')'$. Here and everywhere below the prime denotes the derivative with respect to s and the function $r(s)$ completely determines the surface, see Appendix B. The dimensionless DMI constant $d = D/\sqrt{AK}$ is the only material parameter, which controls the system, and $\Xi = 1 + r^{-2}r'^2 - k_2^2 + d\mathcal{H}$. It is important to note that any solution of Eq. (3) and its energy

$$\begin{aligned} \mathcal{E} = \frac{1}{4} \int_0^\infty & \left[\Theta'^2 + 2\Theta' (d\sin^2\Theta - k_1) + \Xi\sin^2\Theta \right. \\ & \left. - 2k_2 \frac{r'}{r} \sin\Theta\cos\Theta + k_1^2 + k_2^2 \right] r(s) ds \end{aligned} \quad (4)$$

are invariant with respect to the transformation $\Theta \rightarrow \Theta + \pi$, i.e. any solution is doubly degenerate with respect to the replacement $\mathbf{m} \rightarrow -\mathbf{m}$.⁴⁴ Consequently, one can fix the boundary condition $\Theta(0) = \pi$ at the bump center without loss of generality and consider different boundary conditions at the infinity: $\Theta(\infty) = n\pi$ with $n \in \mathbb{Z}$. In (4) and everywhere below we use the normalized energy $\mathcal{E} = E/E_{BP}$, where $E_{BP} = 8\pi AL$ is energy of the Belavin-Polyakov soliton.⁴⁵ The same invariance takes place for the transformation $k_1 \rightarrow -k_1$, $k_2 \rightarrow -k_2$, $d \rightarrow -d$, $\Theta \rightarrow 2\pi - \Theta$. This property is reflected in the symmetry of the diagram of skyrmion states, see Fig. 3.

Following Ref. 41 one can show that topological charge (mapping degree to S^2) of such a radially symmetrical solution on a localized bump reads $Q = \frac{1}{2}[\cos\Theta(\infty) - \cos\Theta(0)]$, see Appendix C for details. It means that only values $Q = 0$ (for odd n) or $Q = 1$ (for even n) are possible. A state with $Q = -1$ appears under the transformation $\mathbf{m} \rightarrow -\mathbf{m}$ applied to the state with $Q = 1$.

Due to the presence of the right-hand-part driving term in Eq. (3) the trivial solutions $\Theta \equiv 0, \pi$ (i.e. $\mathbf{m} = \pm\mathbf{n}$) are generally not possible. It means that even for large anisotropy the magnetization vector deviates from the normal direction, except surfaces with $\mathcal{H} = \text{const}$, e.g. planar films, spherical and minimal surfaces. Such a prediction was previously made in Ref. 39. An analogous driving appears in 1D curvilinear wires and results in curvature induced domain wall motion along the curvature gradient.⁴⁶ Thus, Eq. (3) makes one expect a leading role of the mean curvature gradient in the analogous curvature induced skyrmion motion.

In the planar film limit $k_1 = k_2 \equiv 0$, $\mathcal{H} \equiv 0$ and $r(s) = s$. In this case Eq. (3) is transformed into the well-

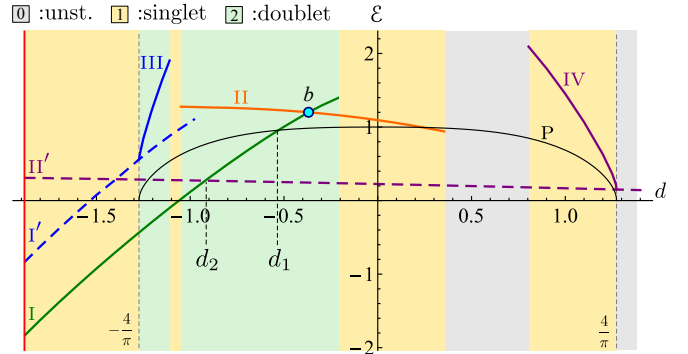


FIG. 2. **Energies of different solutions.** Solid lines I–IV and dashed lines I', II' show energies (4) of topological non-trivial (skyrmion) and trivial states, respectively for the bump with $\mathcal{A} = 2$ and $r_0 = 1$. Energy of the planar skyrmion is shown by the thin line P. States I, II, I', II' are similar to the same name states in Fig. 1. States III and IV correspond to skyrmions whose radius much exceeds the lateral bump size, see Figs. 6, 9. The background filling corresponds to the number of stable skyrmion states, see also Fig. 3.

known^{2,31,34,38} chiral skyrmion equation. Such a planar system is controlled by the only parameter d . There is the critical value $d_0 = 4/\pi$, which separates two ground states, namely the uniform state $\mathbf{m} = \mathbf{n}$ for the case $|d| < d_0$, and helical periodical state for $|d| > d_0$.^{2,31,34,38} For the case $|d| < d_0$ the planar form of Eq. (3) has a stable topological ($Q = 1$) solution – a skyrmion, which has the following features: (i) for a given value of d the skyrmion solution is unique; (ii) the skyrmion energy is always higher than energy of the uniform perpendicular state, i.e. the planar skyrmion is an excitation of the ground state. As we show below, these well-known properties are violated in the general case of the curvilinear defect.

III. GAUSSIAN BUMP

As an example, we consider a class of localized curvilinear defects in form $z(r) = Ae^{-r^2/(2r_0^2)}$. Here amplitudes $A > 0$ and $A < 0$ correspond to bumps that are convex or concave, respectively, and r_0 determines the bump width. In Fig. 1(a) we demonstrate stable equilibrium solutions of Eq. (3) for certain values of parameters. There is a number of principal differences as compared to the planar case:

(i) Topological ($Q = 1$) as well as trivial ($Q = 0$) solutions are generally not unique: for given values of geometrical and material parameters a set of equilibrium magnetization states can appear with a ladder of energy levels. This makes the curvilinear defect conceptually similar to a quantum well with a finite number of discrete energy levels. However, in contrast to the quantum systems the transitions between levels with the same Q are only allowed. Such transitions are expected to be

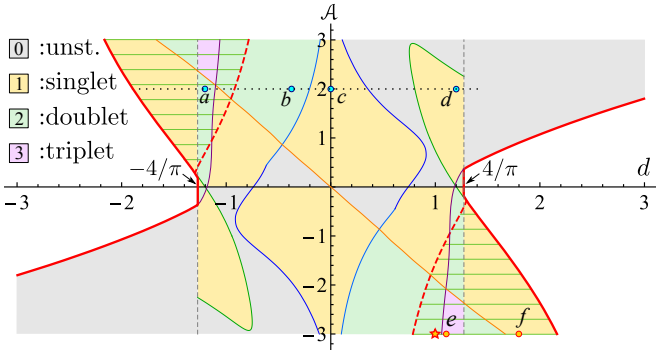


FIG. 3. Diagram of skyrmion states for Gaußian bump with $r_0 = 1$. In the white area the skyrmion solutions does not exist. Number of any other area (see legend) coincides with the number of stable skyrmion solutions. At least one skyrmion solution exists within the gray area ‘0’, however the bump center is a position of unstable equilibrium for it. Within the other areas the corresponding number of skyrmion are pinned at the bump center. The horizontal dashing shows areas where the lowest energy level is skyrmion one. Star marker shows parameters of Fig. 1. The solutions spectra for points $a-f$ are presented in Appendix E. Dotted horizontal line $A = 2$ corresponds to Fig. 2.

accompanied by emission or absorption of magnons.

(ii) The lowest energy level can be topological non-trivial ($Q = 1$). Recently it was shown⁵ that due to nonlocal magnetosatic effects the skyrmion state of a finite size disk can have lower energy as compared to the topologically trivial homogeneous state. Here we thus demonstrate that the same is possible in curvilinear systems due to local interactions only. As a consequence, curvilinear defects arranged in a periodical lattice generate a zero-field skyrmion lattice^{25,26} as a ground state of the system, see Fig. 1(c).

Let us consider skyrmions of small and big radii, which are shown in the Fig. 1 as states I(“1”) and II(“0”), respectively. Their radii⁴⁷ are close to extrema points of the Gauß curvature $\mathcal{K} = k_1 k_2$, which plays an important role in a coupling between topological defects and curvature.^{48,49} Hence, one can expect an important role of the curvature in the skyrmions stabilization. On the other hand, the radius of skyrmion II is of one order of magnitude smaller than radius of the skyrmion, which is stabilized by the intrinsic DMI in a planar film for the same value of d . Thus, the small radius skyrmion is stabilized mostly by the curvature effects,^{41,50–52} while the big radius skyrmion is stabilized due to the simultaneous action of the intrinsic DMI and curvature. Structures similar to the big radius skyrmions were previously observed experimentally in Co/Pd and Co/Pt multilayer films containing an array of curvilinear defects in form of spherical concavities^{53,54} as well as convexes.^{55,56} The topologically trivial state I’ can be treated as a joint state of small and big radii skyrmions, which compensate topological charges of each other. And the state II’ is an intermediate one between uniform $\mathbf{m} = -\mathbf{e}_z$ and

normal $\mathbf{m} = -\mathbf{n}$ states, what reflects the competition between exchange and anisotropy interactions. Note that states I and I’ as well as states II and II’ differ in presence or absence of the small-radius skyrmion at the bump center. In Fig. 1(a) we show only stable solutions with $\Delta\Theta = |\Theta(\infty) - \Theta(0)| \leq \pi$. Solutions with the larger phase incursion, so called skyrmioniums^{34,57} or target skyrmions,^{13,32,38,58,59} are in principle also possible.

The appearance of skyrmions of type I (big radius) and type II (small radius) is a common feature of the considered curvilinear defects, and takes place for concave as well as for convex geometries. In order to illustrate the last statement we show the energies $\mathcal{E}(d)$ for all equilibrium states, which appear for a convex bump, see Fig. 2. For the given geometrical parameters we found numerically all solutions of Eq. (3) with $\Delta\Theta \leq \pi$ for each value d . Then a stability analysis (see Appendix D) was applied for each of the solutions. Finally, four stable topological (skyrmion) solutions (lines I-IV) and two stable non-topological solutions (lines I’ and II’) are found. The magnetization distributions, that correspond to all of these solutions, are shown in Appendix E. Lines I and II correspond to the considered above big (“1”) and small (“0”) radius skyrmions, respectively. Remarkably these states can have equal energies – point b in Fig. 2. This makes the proposed application for the storing of a bit of information more practically relevant: switching between states “0” and “1” can be easily controlled by application of pulse of magnetic field directed along or against the vertical axis.

As well as for the concave geometry (Fig. 1) the big radius skyrmion on a convex bump can have the lowest energy in the system (the range $d < d_2$). It is important to note that there is a range of parameters $-4/\pi < d < d_1$ where a skyrmion on a bump has lower energy than a planar skyrmion for the same d . This implies that flexible enough planar films can spontaneously undergo a skyrmion induced deformation. Such a soliton-induced magnetic film deformation was earlier predicted for cylindrical geometries.^{60–64}

In order to systematize possible skyrmion solutions, that can appear on Gaußian bumps, we build a diagram of skyrmion states, see Fig. 3. We apply the same method as for the case of Fig. 2, but restricting ourselves with skyrmion solutions. The following general features can be established: (i) The range of skyrmions existence widens with increasing of the bump amplitude. (ii) For a wide range of parameters (gray area ‘0’) the skyrmion centered on the bump experiences a displacement instability because the bump center is a position of unstable equilibrium. (iii) In the vicinity of the critical value $d = \pm 4/\pi$ there is a wide area of parameters (the dashed area), where the skyrmion state has the lowest energy in the class of radially symmetrical solutions. If such a skyrmion is the ground state of the system, then one can consider the described bump as a generator of skyrmions. Indeed, a spontaneous formation of the skyrmion is expected due to thermal fluctuations. Apply-

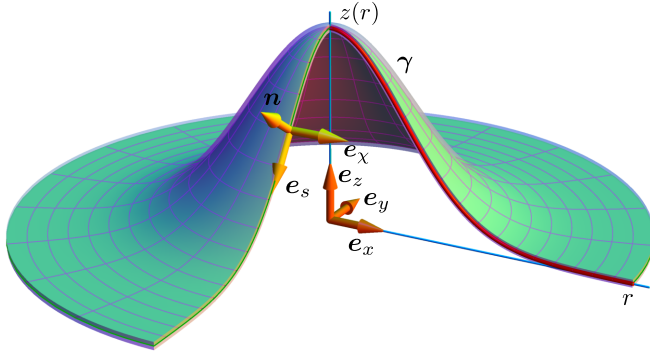


FIG. 4. Details of the geometry. A curvilinear defect is considered as a surface of rotation, which is formed by a complete revolution of the curve $\gamma = re_x + z(r)e_z$ around z -axis. Cartesian $\{e_x, e_y, e_z\}$ and curvilinear $\{e_s, e_x, n\}$ frames of reference are introduced.

ing now a strong enough in-surface spin-polarized current can move the skyrmion from the bump into the planar part of the film. This operation can be then repeated.

IV. CONCLUSIONS

We have generalized the skyrmion equation for the case of an arbitrary surface of rotation. Considering specifically a Gaussian bump we have shown that its skyrmion solution is generally not unique — a discrete ladder of equilibrium skyrmion states appears. We propose to use a suitably shaped curvilinear defect with a doubly degenerate skyrmion state as carrier of a bit of information. We also predict the effect of spontaneous deformation of an elastic magnetic film under skyrmion influence. Finally, we found a wide range of parameters, where a skyrmion pinned on the bump has lower energy than other possible states. This feature can be used for generating of a ground state zero-field skyrmion lattice.

V. ACKNOWLEDGMENTS

V.P.K. acknowledges the Alexander von Humboldt Foundation for the support. This work has been supported by the DFG via SFB 1143 and by ERC within the EU 7th Framework Programme (ERC Grant No. 306277) and the EU FET Programme (FET-Open Grant No. 618083). We acknowledge Prof. Avadh Saxena for fruitful discussions.

Appendix A: Geometrical properties of a surface of revolution

Curvilinear properties of the considered surface of rotation (see Fig. 4) are completely determined by two prin-

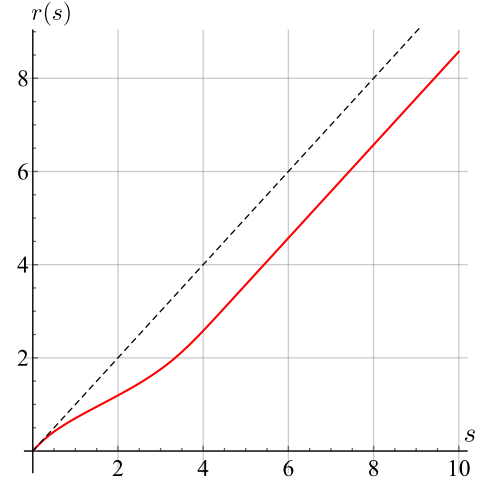


FIG. 5. Arc length parameterization. Dependence $r(s)$ for the Gaussian bump $z(r) = \mathcal{A}e^{-r^2/(2r_0^2)}$ with $\mathcal{A} = 3$ and $r_0 = 1$.

cipal curvatures

$$k_1(r) = \frac{z''(r)}{[1 + z'(r)^2]^{3/2}}, \quad k_2(r) = \frac{z'(r)}{r\sqrt{1 + z'(r)^2}}. \quad (\text{A1})$$

Here k_1 is curvature of γ while k_2 is curvature of the curve created by the section of the surface with the plane perpendicular to γ at each given point. For a surface of rotation the principal curvatures are not independent: for the known k_1 the curvature k_2 can be found as a solution of differential equation $rk'_2(r) + k_2(r) = k_1(r)$ with the initial condition $k_2(0) = k_1(0)$. Principal curvatures are invariants of the surface, so they can be considered as functions of the point.

In the following it is convenient to use the natural parameter s (the arc length along γ) instead of parameter r . The functional dependence $r = r(s)$ between the parameters is determined by differential equation $r'(s)\sqrt{1 + z'_r(r(s))^2} = 1$ supplemented with the initial condition $r(0) = 0$. An example of the dependence $r(s)$ for a Gaussian bump is shown in Fig. 5. Function $r(s)$ completely determines curvilinear properties of the surface:

$$k_1(s) = \frac{r''}{\sqrt{1 - r'^2}}, \quad k_2(s) = -\frac{\sqrt{1 - r'^2}}{r}. \quad (\text{A2})$$

From (A2) one obtains the following useful properties

$$\mathcal{K} = -r''/r, \quad [k_1(s) - k_2(s)]r' = k'_2(s)r. \quad (\text{A3})$$

Appendix B: Equilibrium solutions

Equilibrium solutions are determined by set of equations

$$\frac{\delta E}{\delta \theta} = 0, \quad \frac{\delta E}{\delta \phi} = 0, \quad (\text{B1})$$

where the energy functional E is defined in (1). Exchange energy density for an arbitrary curvilinear film reads^{39,40}

$$\mathcal{E}_{\text{ex}} = [\nabla\theta - \boldsymbol{\Gamma}]^2 + [\sin\theta(\nabla\phi - \boldsymbol{\Omega}) - \cos\theta\partial_\phi\boldsymbol{\Gamma}]^2. \quad (\text{B2})$$

Here $\boldsymbol{\Omega}$ is vector of spin connection and $\boldsymbol{\Gamma} = \|h_{\alpha\beta}\| \cdot \boldsymbol{\varepsilon}$, where $\|h_{\alpha\beta}\|$ is Weingarten map. For details see Refs. 41, 65, and 66. Substituting into the total energy (1) the contributions from the exchange energy (B2), DMI \mathcal{E}_{D} together with the easy-normal anisotropy contribution one can write equations (B1) in the following expanded form

$$\begin{aligned} & \Delta\theta - \sin\theta\cos\theta [1 + (\nabla\phi - \boldsymbol{\Omega})^2 - (\partial_\phi\boldsymbol{\Gamma})^2 + d\mathcal{H}] \\ & - \nabla \cdot \boldsymbol{\Gamma} + \cos 2\theta(\nabla\phi - \boldsymbol{\Omega}) \cdot \partial_\phi\boldsymbol{\Gamma} + d\sin^2\theta\nabla \cdot \boldsymbol{\varepsilon} = 0, \\ & \nabla \cdot [\sin^2\theta(\nabla\phi - \boldsymbol{\Omega})] - \sin\theta\cos\theta [(\nabla\phi - \boldsymbol{\Omega}) \cdot \boldsymbol{\Gamma} + \nabla \cdot \partial_\phi\boldsymbol{\Gamma}] \\ & + \sin^2\theta[2(\nabla\theta \cdot \partial_\phi\boldsymbol{\Gamma}) - \boldsymbol{\Gamma} \cdot \partial_\phi\boldsymbol{\Gamma} - d(\nabla\theta \cdot \boldsymbol{\varepsilon})] = 0. \end{aligned} \quad (\text{B3})$$

For the case of the considered surface of rotation the vector of spin connection is $\boldsymbol{\Omega} = -\mathbf{e}_\chi r'/r$, and $\boldsymbol{\Gamma} = k_1 \cos\phi \mathbf{e}_s + k_2 \sin\phi \mathbf{e}_\chi$. In this case one can see that Eqs. (B3) have solution $\phi = \Phi = 0, \pi$, and $\theta = \Theta(s)$, wherein the second equation in (B3) becomes an identity while the first one obtains the form

$$\Delta_s\Theta - \sin\Theta\cos\Theta\Xi + \mathcal{C}\frac{r'}{r}(d - 2k_2)\sin^2\Theta = \mathcal{C}\mathcal{H}'. \quad (\text{B4})$$

Constant $\mathcal{C} = \cos\Phi = \pm 1$ determines sign of the radial component $m_s = \mathcal{C}\sin\Theta$, while the azimuthal component $m_\chi = 0$ is absent. In this case without loss of generality one can fix the value $\mathcal{C} = +1$ by expanding the range of values of function $\Theta(s)$ to the full circumference $\Theta \in \mathbb{R}$.

Note, that such a simple solution is possible for the interfacing DMI, while for another types of DMI the set of equations (B3) can not be generally uncoupled.

Appendix C: Topological charge calculation

Let us calculate topological charge Q – degree of the mapping to sphere S^2 :

$$Q = \frac{1}{4\pi} \int \mathcal{J} ds. \quad (\text{C1})$$

Here the mapping Jacobian \mathcal{J} reads⁴¹

$$\begin{aligned} \mathcal{J} = & -\sin\theta \mathbf{n} \cdot [(\nabla\theta - \boldsymbol{\Gamma}) \times (\nabla\phi - \boldsymbol{\Omega})] \\ & + \cos\theta \mathbf{n} \cdot [\nabla\theta \times \partial_\phi\boldsymbol{\Gamma}] - \cos\theta \mathcal{K}, \end{aligned} \quad (\text{C2})$$

where $\boldsymbol{\Gamma}$ and $\boldsymbol{\Omega}$ are defined in the previous section. For the case of solution $\theta = \Theta(s)$ and $\phi = 0, \pi$ determined on the considered surface of rotation one has $\nabla\theta = \mathbf{e}_s\Theta'$, $\nabla\phi = \mathbf{0}$, $\boldsymbol{\Gamma} = \mathcal{C}k_1\mathbf{e}_s$, $\partial_\phi\boldsymbol{\Gamma} = \mathcal{C}k_2\mathbf{e}_\chi$ and $\boldsymbol{\Omega} = -\mathbf{e}_\chi r'/r$.

The substitution into (C2) with the subsequent integration (C1) results in

$$Q = \frac{1}{2} [r'(s)\cos\Theta(s)] \Big|_0^\infty = \frac{1}{2} \frac{\cos\Theta(r)}{\sqrt{1 + z'(r)^2}} \Big|_0^\infty. \quad (\text{C3})$$

When integrating (C1) one should use the properties (A3). For a smooth and localized curvilinear defect one has $z'(0) = z'(\infty) = 0$, thus (C3) result in the common formula

$$Q = \frac{1}{2} [\cos\Theta(\infty) - \cos\Theta(0)]. \quad (\text{C4})$$

Appendix D: Stability analysis

Here we consider stability of the obtained stationary solutions Θ and Φ with respect to infinitesimal deviations:

$$\theta = \Theta + \vartheta, \quad \phi = \Phi + \varphi/\sin\Theta, \quad (\text{D1})$$

where $|\vartheta| \ll 1$ and $|\varphi| \ll 1$. In this case the total normalized energy (1) can be presented in form $\mathcal{E} \approx \mathcal{E}_0 + \epsilon$, where $\mathcal{E}_0 = \mathcal{E}[\Theta, \Phi]$ is energy of the unperturbed state, and harmonic part of the energy increase reads

$$\epsilon = \frac{1}{8\pi} \int \boldsymbol{\Psi}^T \hat{\mathbf{H}} \boldsymbol{\Psi} ds. \quad (\text{D2})$$

Here $\boldsymbol{\Psi} = (\vartheta, \varphi)^T$ and

$$\hat{\mathbf{H}} = \begin{pmatrix} -\Delta + U_1 & W\partial_\chi \\ -W\partial_\chi & -\Delta + U_2 \end{pmatrix}. \quad (\text{D3})$$

The Laplace operator has the form $\Delta = \Delta_s + r^{-2}\partial_{\chi\chi}^2$ and potentials are as follows

$$\begin{aligned} U_1 &= \cos 2\Theta\Xi - \mathcal{C}\frac{r'}{r}(d - 2k_2)\sin 2\Theta, \\ U_2 &= \cos^2\Theta\Xi - \Theta'^2 + k_2^2 - k_1^2 - \mathcal{C}(d - 2k_1)\Theta' \\ &\quad - \mathcal{C}\frac{r'}{r}(d - 2k_2)\sin\Theta\cos\Theta, \\ W &= 2\frac{r'}{r^2}\cos\Theta - \frac{\mathcal{C}}{r}(d - 2k_2)\sin\Theta. \end{aligned} \quad (\text{D4})$$

Using the Fourier series expansion

$$\begin{aligned} \vartheta(s, \chi) &= \frac{f_0(s)}{2} + \sum_{\mu \neq 0} [f_\mu(s)\cos\mu\chi + \bar{f}_\mu(s)\sin\mu\chi], \\ \varphi(s, \chi) &= \frac{\bar{g}_0(s)}{2} + \sum_{\mu \neq 0} [\bar{g}_\mu(s)\cos\mu\chi + g_\mu(s)\sin\mu\chi] \end{aligned} \quad (\text{D5})$$

one can present energy (D2) in form

$$\epsilon = \frac{1}{8} \sum_\mu \int r(s) [\boldsymbol{\psi}_\mu^T \hat{\mathcal{H}}_\mu \boldsymbol{\psi}_\mu + \bar{\boldsymbol{\psi}}_\mu^T \hat{\mathcal{H}}_{-\mu} \bar{\boldsymbol{\psi}}_\mu] ds, \quad (\text{D6})$$

where $\mu \in \mathbb{Z}$, $\psi_\mu = (f_\mu, g_\mu)^\text{T}$, $\bar{\psi}_\mu = (\bar{f}_\mu, \bar{g}_\mu)^\text{T}$ and

$$\hat{\mathcal{H}}_\mu = \begin{pmatrix} -\Delta_s + \frac{\mu^2}{r^2} + U_1 & \mu W \\ \mu W & -\Delta_s + \frac{\mu^2}{r^2} + U_2 \end{pmatrix}. \quad (\text{D7})$$

Stationary solution (Θ, Φ) corresponds to a minimum of energy iff $\epsilon > 0$ for any ψ_μ and $\bar{\psi}_\mu$. Taking into account that eigenvalues $\lambda_i^{(\mu)}$ of operator $\hat{\mathcal{H}}_\mu$ do not depend on sign of μ , one can state that positiveness of all $\lambda_i^{(\mu)}$ for all i is a sufficient condition for the energy minimum, i.e. stability.

In order to check stability of a solution (Θ, Φ) we found numerically the lowest eigenvalues $\Lambda^{(\mu)} = \min_i \lambda_i^{(\mu)}$ of

operators $\hat{\mathcal{H}}_\mu$, with $\mu = 0, 1, \dots, 4$. If all $\Lambda^{(\mu)} > 0$, we conclude that the solution (Θ, Φ) is stable. In case of the skyrmion solution one can say that the bump effectively generates pinning potential. If $\Lambda^{(1)} < 0$ and $\Lambda^{(\mu \neq 1)} > 0$, then we conclude that the bump effectively generates repulsing potential. One can say about displacement instability in this case. For the cases $\Lambda^{(0)} < 0$ and $\Lambda^{(2)} < 0$ one can say about radial³² and elliptical^{32,67} instability, respectively.

Appendix E: Examples of possible equilibrium magnetization states

Here we present spectra of stable solutions of Eq. (3), which correspond to the points *a*–*f* in Fig. 3.

* vkravchuk@bitp.kiev.ua

- ¹ Naoto Nagaosa and Yoshinori Tokura, “Topological properties and dynamics of magnetic skyrmions,” *Nature Nanotechnology* **8**, 899–911 (2013).
- ² A O Leonov, T L Monchesky, N Romming, A Kubetzka, A N Bogdanov, and R Wiesendanger, “The properties of isolated chiral skyrmions in thin magnetic films,” *New J. Phys.* **18**, 065003 (2016).
- ³ Roland Wiesendanger, “Nanoscale magnetic skyrmions in metallic films and multilayers: a new twist for spintronics,” *Nature Reviews Materials* **1**, 16044 (2016).
- ⁴ Albert Fert, Vincent Cros, and Joao Sampaio, “Skyrmions on the track,” *Nature Nanotechnology* **8**, 152–156 (2013).
- ⁵ J. Sampaio, V. Cros, S. Rohart, A. Thiaville, and A. Fert, “Nucleation, stability and current-induced motion of isolated magnetic skyrmions in nanostructures,” *Nature Nanotechnology* **8**, 839–844 (2013).
- ⁶ R. Tomasello, E. Martinez, R. Zivieri, L. Torres, M. Carpentieri, and G. Finocchio, “A strategy for the design of skyrmion racetrack memories,” *Scientific Reports* **4**, 6784 (2014).
- ⁷ Xichao Zhang, G. P. Zhao, Hans Fangohr, J. Ping Liu, W. X. Xia, J. Xia, and F. J. Morvan, “Skyrmion-skyrmion and skyrmion-edge repulsions in skyrmion-based racetrack memory,” *Scientific Reports* **5**, 7643 (2015).
- ⁸ Stefan Krause and Roland Wiesendanger, “Spintronics: Skyrmionics gets hot,” *Nature Materials* **15**, 493–494 (2016).
- ⁹ Wang Kang, Yangqi Huang, Chentian Zheng, Weifeng Lv, Na Lei, Youguang Zhang, Xichao Zhang, Yan Zhou, and Weisheng Zhao, “Voltage controlled magnetic skyrmion motion for racetrack memory,” *Scientific Reports* **6**, 23164 (2016).
- ¹⁰ Jan Müller, “Magnetic skyrmions on a two-lane racetrack,” *New Journal of Physics* **19**, 025002 (2017).
- ¹¹ Niklas Romming, Christian Hanneken, Matthias Menzel, Jessica E. Bickel, Boris Wolter, Kirsten von Bergmann, Andr Kubetzka, and Roland Wiesendanger, “Writing and deleting single magnetic skyrmions,” *Science* **341**, 636–639 (2013).
- ¹² W. Jiang, P. Upadhyaya, W. Zhang, G. Yu, M. B. Jungfleisch, F. Y. Fradin, J. E. Pearson, Y. Tserkovnyak, K. L. Wang, O. Heinonen, S. G. E. te Velthuis, and A. Hoffmann, “Blowing magnetic skyrmion bubbles,” *Science* **349**, 283–286 (2015).
- ¹³ Marijan Beg, Rebecca Carey, Weiwei Wang, David Cortés-Ortuño, Mark Vousden, Marc-Antonio Bisotti, Maximilian Albert, Dmitri Chernyshenko, Ondrej Hovorka, Robert L. Stamps, and Hans Fangohr, “Ground state search, hysteretic behaviour, and reversal mechanism of skyrmionic textures in confined helimagnetic nanostructures,” *Scientific Reports* **5**, 17137 (2015).
- ¹⁴ Felix Büttner, C. Moutafis, M. Schneider, B. Krüger, C. M. Günther, J. Geilhufe, C. v. Korff Schmising, J. Mohanty, B. Pfau, S. Schaffert, A. Bisig, M. Foerster, T. Schulz, C. A. F. Vaz, J. H. Franken, H. J. M. Swagten, M. Kläui, and S. Eisebitt, “Dynamics and inertia of skyrmionic spin structures,” *Nat Phys* **11**, 225–228 (2015).
- ¹⁵ S. Mühlbauer, B. Binz, F. Jonietz, C. Pfleiderer, A. Rosch, A. Neubauer, R. Georgii, and P. Böni, “Skyrmion lattice in a chiral magnet,” *Science* **323**, 915–919 (2009).
- ¹⁶ X. Z. Yu, Y. Onose, N. Kanazawa, J. H. Park, J. H. Han, Y. Matsui, N. Nagaosa, and Y. Tokura, “Real-space observation of a two-dimensional skyrmion crystal,” *Nature* **465**, 901–904 (2010).
- ¹⁷ X. Z. Yu, N. Kanazawa, Y. Onose, K. Kimoto, W. Z. Zhang, S. Ishiwata, Y. Matsui, and Y. Tokura, “Near room-temperature formation of a skyrmion crystal in thin-films of the helimagnet fege,” *Nat Mater* **10**, 106–109 (2011).
- ¹⁸ P. Milde, D. Kohler, J. Seidel, L. M. Eng, A. Bauer, A. Chacon, J. Kindervater, S. Muhlbauer, C. Pfleiderer, S. Buhrandt, and et al., “Unwinding of a skyrmion lattice by magnetic monopoles,” *Science* **340**, 1076–1080 (2013).
- ¹⁹ U. K. Rößler, A. N. Bogdanov, and C. Pfleiderer, “Spontaneous skyrmion ground states in magnetic metals,” *Nature* **442**, 797–801 (2006).
- ²⁰ Minhyea Lee, W. Kang, Y. Onose, Y. Tokura, and N. P. Ong, “Unusual hall effect anomaly in MnSi under pressure,” *Physical Review Letters* **102** (2009), 10.1103/physrevlett.102.186601.
- ²¹ A. Neubauer, C. Pfleiderer, B. Binz, A. Rosch, R. Ritz, P. G. Niklowitz, and P. Bni, “Topological hall effect in the a phase of MnSi,” *Phys. Rev. Lett.* **102**, 186602 (2009).

- ²² N. Kanazawa, Y. Onose, T. Arima, D. Okuyama, K. Ohoyama, S. Wakimoto, K. Kakurai, S. Ishiwata, and Y. Tokura, “Large topological hall effect in a short-period helimagnet MnGe,” *Phys. Rev. Lett.* **106** (2011), 10.1103/physrevlett.106.156603.
- ²³ Yufan Li, N. Kanazawa, X. Z. Yu, A. Tsukazaki, M. Kawasaki, M. Ichikawa, X. F. Jin, F. Kagawa, and Y. Tokura, “Robust formation of skyrmions and topological hall effect anomaly in epitaxial thin films of MnSi,” *Phys. Rev. Lett.* **110**, 117202 (2013).
- ²⁴ Gong Chen, Arantzazu Mascaraque, Alpha T. N’Diaye, and Andreas K. Schmid, “Room temperature skyrmion ground state stabilized through interlayer exchange coupling,” *Applied Physics Letters* **106**, 242404 (2015).
- ²⁵ Stefan Heinze, Kirsten von Bergmann, Matthias Menzel, Jens Brede, Andre Kubetzka, Roland Wiesendanger, Gustav Bihlmayer, and Stefan Blugel, “Spontaneous atomic-scale magnetic skyrmion lattice in two dimensions,” *Nat Phys* **7**, 713–718 (2011).
- ²⁶ N. Kanazawa, J.-H. Kim, D. S. Inosov, J. S. White, N. Egetenmeyer, J. L. Gavilano, S. Ishiwata, Y. Onose, T. Arima, B. Keimer, and Y. Tokura, “Possible skyrmion-lattice ground state in the b20 chiral-lattice magnet mnge as seen via small-angle neutron scattering,” *Phys. Rev. B* **86**, 134425 (2012).
- ²⁷ Yangqi Huang, Wang Kang, Xichao Zhang, Yan Zhou, and Weisheng Zhao, “Magnetic skyrmion-based synaptic devices,” *Nanotechnology* **28**, 08LT02 (2017).
- ²⁸ Diana Prychynenko, Matthias Sitte, Kai Litzius, Benjamin Krger, George Bourianoff, Mathias Klui, Jairo Sinova, and Karin Everschor-Sitte, “A magnetic skyrmion as a non-linear resistive element - a potential building block for reservoir computing,” [1702.04298v2](https://arxiv.org/abs/1702.04298v2).
- ²⁹ Zhezhi He and Deliang Fan, “Developing all-skyrmion spiking neural network,” [1705.02995v1](https://arxiv.org/abs/1705.02995v1).
- ³⁰ A. N. Bogdanov and D. A. Yablonski, “Thermodynamically stable “vortices” in magnetically ordered crystals. the mixed state of magnets,” *Zh. Eksp. Teor. Fiz.* **95**, 178–182 (1989).
- ³¹ A. Bogdanov and A. Hubert, “Thermodynamically stable magnetic vortex states in magnetic crystals,” *Journal of Magnetism and Magnetic Materials* **138**, 255–269 (1994).
- ³² A. Bogdanov and A. Hubert, “The stability of vortex-like structures in uniaxial ferromagnets,” *Journal of Magnetism and Magnetic Materials* **195**, 182–192 (1999).
- ³³ A. Bogdanov and U. Rößler, “Chiral symmetry breaking in magnetic thin films and multilayers,” *Physical Review Letters* **87**, 037203 (2001).
- ³⁴ Stavros Komineas and Nikos Papanicolaou, “Skyrmion dynamics in chiral ferromagnets,” *Phys. Rev. B* **92** (2015), 10.1103/physrevb.92.064412.
- ³⁵ A. Crépieux and C. Lacroix, “Dzyaloshinsky-Moriya interactions induced by symmetry breaking at a surface,” *Journal of Magnetism and Magnetic Materials* **182**, 341–349 (1998).
- ³⁶ André Thiaville, Stanislas Rohart, Émilie Jué, Vincent Cros, and Albert Fert, “Dynamics of Dzyaloshinskii domain walls in ultrathin magnetic films,” *EPL (Europhysics Letters)* **100**, 57002 (2012).
- ³⁷ Hongxin Yang, André Thiaville, Stanislas Rohart, Albert Fert, and Mairbek Chshiev, “Anatomy of Dzyaloshinskii-Moriya interaction at Co/Pt interfaces,” *Phys. Rev. Lett.* **115**, 267210 (2015).
- ³⁸ S. Rohart and A. Thiaville, “Skyrmion confinement in ultrathin film nanostructures in the presence of Dzyaloshinskii-Moriya interaction,” *Physical Review B* **88**, 184422 (2013).
- ³⁹ Yuri Gaididei, Volodymyr P. Kravchuk, and Denis D. Sheka, “Curvature effects in thin magnetic shells,” *Phys. Rev. Lett.* **112**, 257203 (2014).
- ⁴⁰ Denis D. Sheka, Volodymyr P. Kravchuk, and Yuri Gaididei, “Curvature effects in statics and dynamics of low dimensional magnets,” *Journal of Physics A: Mathematical and Theoretical* **48**, 125202 (2015).
- ⁴¹ Volodymyr P. Kravchuk, Ulrich K. Rößler, Oleksii M. Volkov, Denis D. Sheka, Jeroen van den Brink, Denys Makarov, Hagen Fuchs, Hans Fangohr, and Yuri Gaididei, “Topologically stable magnetization states on a spherical shell: Curvature-stabilized skyrmions,” *Phys. Rev. B* **94**, 144402 (2016).
- ⁴² In other words the magnetostatic contribution is replaced by an effective easy-surface anisotropy,^{68–71} which simply results in a shift of the anisotropy constant K .
- ⁴³ Note that the sign of each of the quantities \mathcal{H} and D separately is not physically fixed, because it is determined by the chosen direction of the normal vector \mathbf{n} .
- ⁴⁴ If solution \mathbf{m} is stable then solution $-\mathbf{m}$ is also stable, see Appendix D.
- ⁴⁵ A. A. Belavin and A. M. Polyakov, “Metastable states of a 2D isotropic ferromagnet,” *JETP Lett.* **22**, 245 (1975).
- ⁴⁶ Kostiantyn V. Yershov, Volodymyr P. Kravchuk, Denis D. Sheka, and Yuri Gaididei, “Curvature-induced domain wall pinning,” *Phys. Rev. B* **92**, 104412 (2015).
- ⁴⁷ Skyrmion radius R is determined as solution of equation $\cos \Theta(R) = 0$. For the parameters of Fig. 1 the small and big skyrmion radii are $R_{\text{sml}} \approx 0.14$ and $R_{\text{big}} \approx 3.7$, respectively; $\mathcal{K}(s)$ has extreme points $s_1 = 0$ and $s_2 \approx 3.3$.
- ⁴⁸ Vincenzo Vitelli and Ari M. Turner, “Anomalous coupling between topological defects and curvature,” *Phys. Rev. Lett.* **93**, 215301 (2004).
- ⁴⁹ Ari M. Turner, Vincenzo Vitelli, and David R. Nelson, “Vortices on curved surfaces,” *Rev. Mod. Phys.* **82**, 1301–1348 (2010).
- ⁵⁰ V.L. Carvalho-Santos, R.G. Elias, D. Altbir, and J.M. Fonseca, “Stability of skyrmions on curved surfaces in the presence of a magnetic field,” *Journal of Magnetism and Magnetic Materials* **391**, 179–183 (2015).
- ⁵¹ V.L. Carvalho-Santos, F.A. Apolonio, and N.M. Oliveira-Neto, “On geometry-dependent vortex stability and topological spin excitations on curved surfaces with cylindrical symmetry,” *Physics Letters A* **377**, 1308–1316 (2013).
- ⁵² Priscila S.C. Vilas-Boas, Ricardo G. Elias, Dora Altbir, Jakson M. Fonseca, and Vagson L. Carvalho-Santos, “Topological magnetic solitons on a paraboloidal shell,” *Physics Letters A* **379**, 47–53 (2015).
- ⁵³ D. Makarov, L. Baraban, I. L. Guhr, J. Boneberg, H. Schift, J. Gobrecht, G. Schatz, P. Leiderer, and M. Albrecht, “Arrays of magnetic nanoindentations with perpendicular anisotropy,” *Appl. Phys. Lett.* **90**, 093117 (2007).
- ⁵⁴ D. Makarov, P. Krone, D. Lantiat, C. Schulze, A. Liebig, C. Brombacher, M. Hietschold, S. Hermann, C. Laberty, D. Gross, and M. Albrecht, “Magnetization reversal in arrays of magnetic nanoporations,” *Magnetics, IEEE Transactions on* **45**, 3515–3518 (2009).
- ⁵⁵ Christoph Brombacher, Marc Saitner, Christian Pfahler, Alfred Plett, Paul Ziemann, Denys Makarov, Daniel Assmann, Martin H Siekman, Leon Abelmann, and Manfred

- Albrecht, "Tailoring particle arrays by isotropic plasma etching: an approach towards percolated perpendicular media," *Nanotechnology* **20**, 105304 (2009).
- ⁵⁶ Robert Streubel, Peter Fischer, Florian Kronast, Volodymyr P. Kravchuk, Denis D. Sheka, Yuri Gaididei, Oliver G. Schmidt, and Denys Makarov, "Magnetism in curved geometries (topical review)," *Journal of Physics D: Applied Physics* **49**, 363001 (2016).
- ⁵⁷ M. Finazzi, M. Savoini, A. R. Khorsand, A. Tsukamoto, A. Itoh, L. Duò, A. Kirilyuk, Th. Rasing, and M. Ezawa, "Laser-induced magnetic nanostructures with tunable topological properties," *Phys. Rev. Lett.* **110**, 177205 (2013).
- ⁵⁸ Yan Liu, Haifeng Du, Min Jia, and An Du, "Switching of a target skyrmion by a spin-polarized current," *Physical Review B* **91**, 094425 (2015).
- ⁵⁹ A. O. Leonov, U. K. Rößler, and M. Mostovoy, "Target-skyrmions and skyrmion clusters in nanowires of chiral magnets," *EPJ Web of Conferences* **75**, 05002 (2014).
- ⁶⁰ R. Dandoloff, S. Villain-Guillot, A. Saxena, and A. R. Bishop, "Violation of self-duality for topological solitons due to soliton-soliton interaction on a cylindrical geometry," *Phys. Rev. Lett.* **74**, 813–815 (1995).
- ⁶¹ S. Villain-Guillot, R. Dandoloff, A. Saxena, and A. R. Bishop, "Topological solitons and geometrical frustration," *Phys. Rev. B* **52**, 6712–6722 (1995).
- ⁶² A. Saxena and R. Dandoloff, "Curvature-induced geometrical frustration in magnetic systems," *Phys. Rev. B* **55**, 11049–11051 (1997).
- ⁶³ A. Saxena, R. Dandoloff, and T. Lookman, "Deformable curved magnetic surfaces," *Physica A: Statistical and Theoretical Physics* **261**, 13–25 (1998).
- ⁶⁴ A. Saxena and R. Dandoloff, "Heisenberg spins on a cylinder in an axial magnetic field," *Phys. Rev. B* **58**, R563–R566 (1998).
- ⁶⁵ Randall Kamien, "The geometry of soft materials: a primer," *Reviews of Modern Physics* **74**, 953–971 (2002).
- ⁶⁶ Mark J. Bowick and Luca Giomi, "Two-dimensional matter: order, curvature and defects," *Advances in Physics* **58**, 449–563 (2009).
- ⁶⁷ A. Bogdanov and A. Hubert, "The properties of isolated magnetic vortices," *physica status solidi (b)* **186**, 527–543 (1994).
- ⁶⁸ Valery Slastikov, "Micromagnetism of thin shells," *Mathematical Models and Methods in Applied Sciences* **15**, 1469–1487 (2005).
- ⁶⁹ G. Gioia and R. D. James, "Micromagnetics of very thin films," *Proc. R. Soc. Lond. A* **453**, 213–223 (1997).
- ⁷⁰ R. Kohn and V. Slastikov, "Effective dynamics for ferromagnetic thin films: a rigorous justification," *Proc. R. Soc. A* **461**, 143–154 (2005).
- ⁷¹ Robert V. Kohn and Valeriy V. Slastikov, "Another thin-film limit of micromagnetics," *Archive for Rational Mechanics and Analysis* **178**, 227–245 (2005).

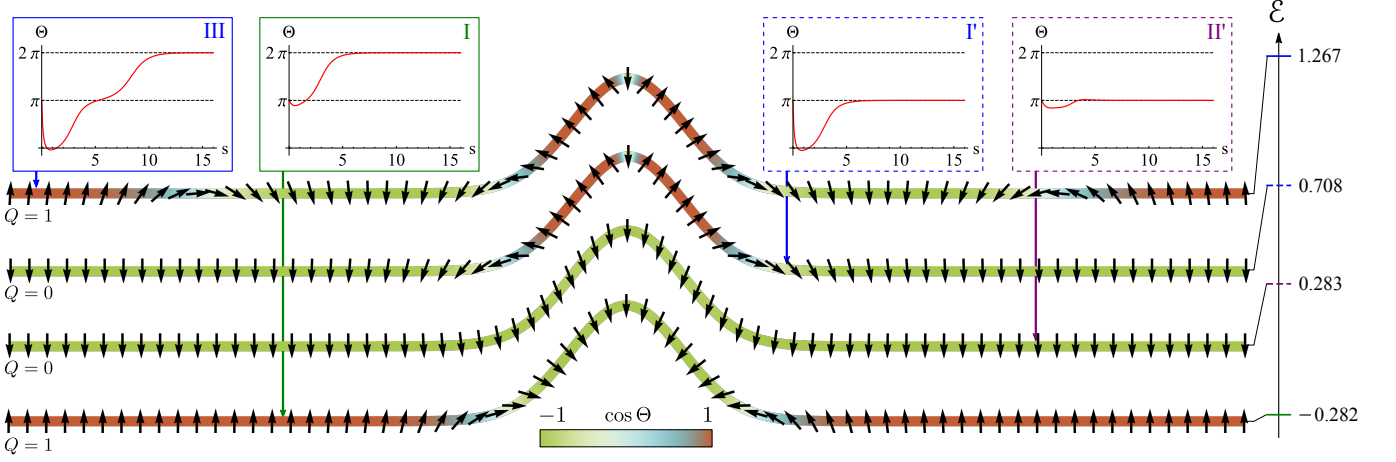


FIG. 6. Spectrum of equilibrium magnetization states, which correspond to point “a” in Fig. 3 — $\mathcal{A} = 2$, $r_0 = 1$, $d = -1.2$. The lowest I and the highest III energy skyrmions correspond to lines I and III in Fig. 2, respectively. Non-topological solutions I' and II' correspond to the lines I' and II', respectively.

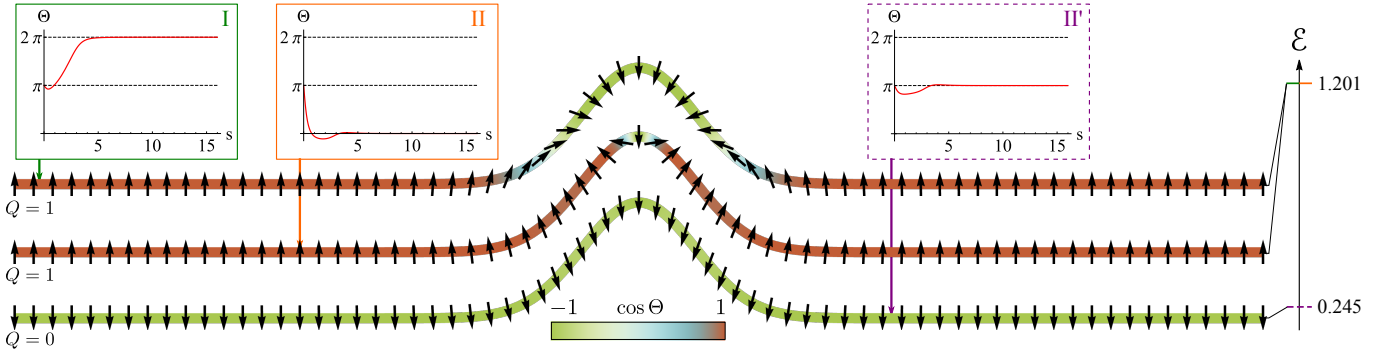


FIG. 7. Spectrum of equilibrium magnetization states, which correspond to point “b” in Figs. 3, 2 — $\mathcal{A} = 2$, $r_0 = 1$, $d = -0.368$. The big I and small II radius skyrmions correspond to lines I and II in Fig. 2, respectively. Non-topological solution II' corresponds to the line II'.

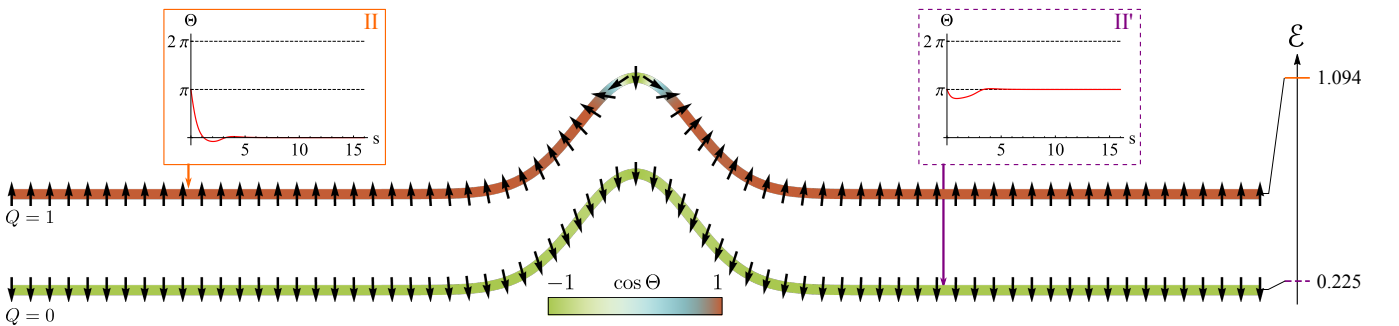


FIG. 8. Spectrum of equilibrium magnetization states, which correspond to point “c” in Fig. 3 — $\mathcal{A} = 2$, $r_0 = 1$, $d = 0$. The curvature stabilized skyrmion II and non-topological solution II' correspond to lines II and II' in Fig. 2, respectively.

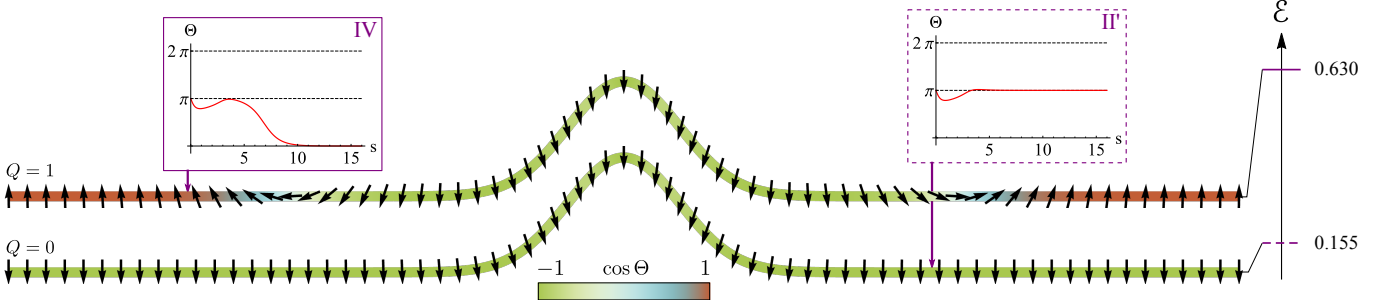


FIG. 9. Spectrum of equilibrium magnetization states, which correspond to point “d” in Fig. 3 — $\mathcal{A} = 2$, $r_0 = 1$, $d = 1.2$. Skyrmion IV and non-topological solution II’ correspond to lines IV and II’ in Fig. 2, respectively.

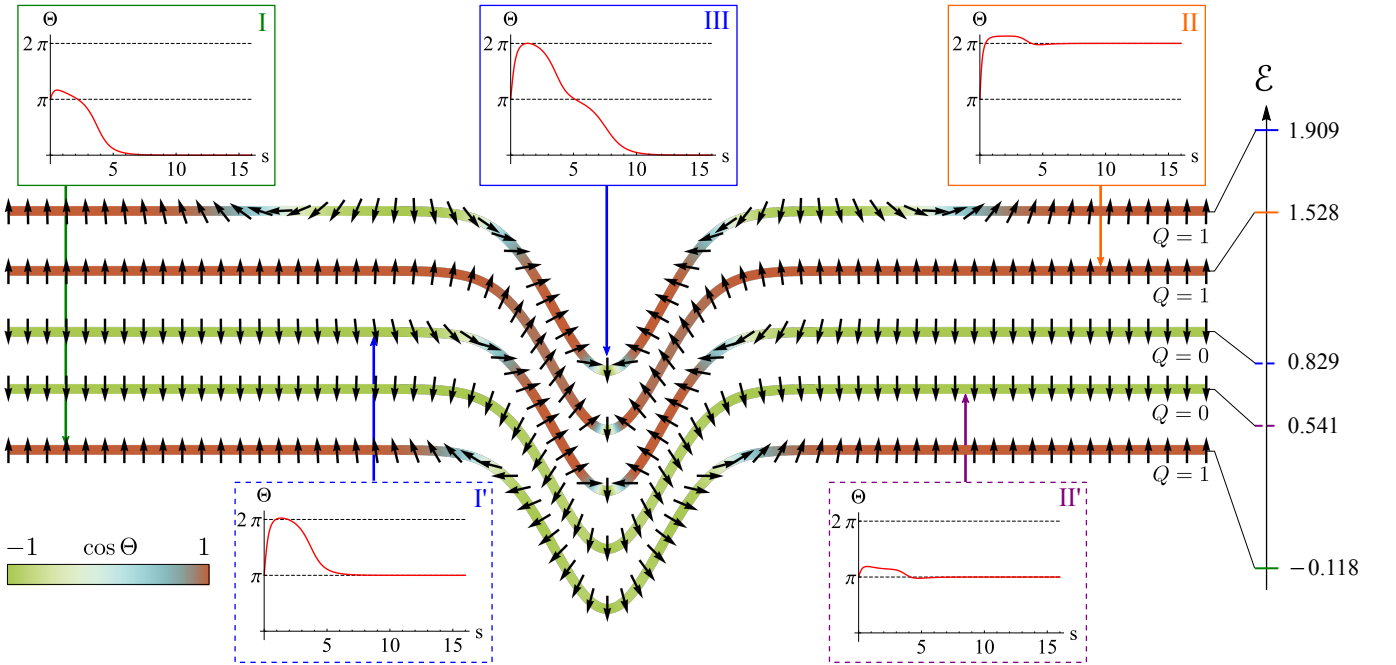


FIG. 10. Spectrum of equilibrium magnetization states, which correspond to point “e” in Fig. 3 — $\mathcal{A} = -3$, $r_0 = 1$, $d = 1.1$.

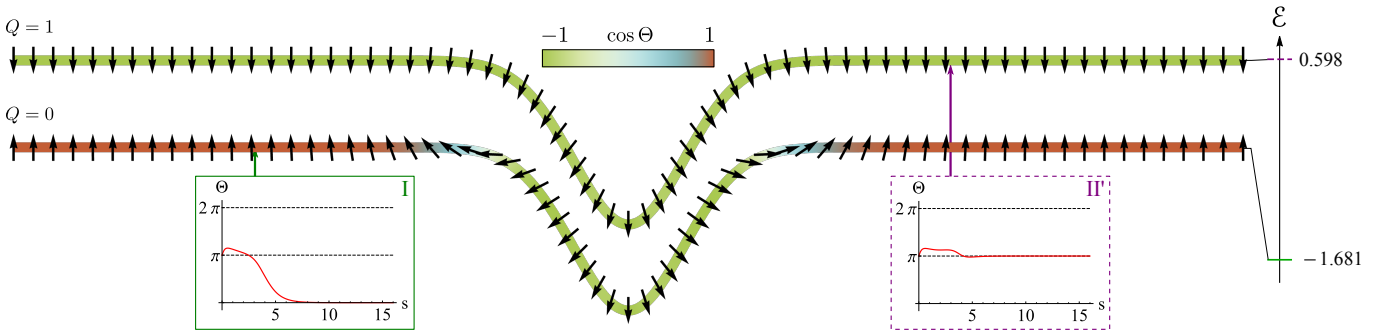


FIG. 11. Spectrum of equilibrium magnetization states, which correspond to point “f” in Fig. 3 — $\mathcal{A} = -3$, $r_0 = 1$, $d = 1.8$.